

Combining UWB with Time Reversal for improved communication and positioning

Luca De Nardis · Jocelyn Fiorina · Dorin Panaitopol ·
Maria-Gabriella Di Benedetto

© Springer Science+Business Media, LLC 2011

Abstract This work investigates the use of Time Reversal (TR) applied to UWB systems for communication and positioning applications. Potential performance boosts, that are achievable over a single UWB communication link by the sole adoption of TR, are investigated. In the case of multiuser UWB communications, it is shown that TR modifies the distribution of Multi User Interference (MUI) and that further performance improvement can be obtained by adapting the receiver to the specific MUI distribution characteristics. As regards UWB positioning, an enhancement in position estimation accuracy can be achieved when TR reinforces DOA estimation thanks to increased robustness to decreased homogeneity in the propagation medium.

Keywords UWB · Time Reversal · Positioning · DOA · MUI distribution

1 Introduction

Time Reversal (TR) has been successfully used for many years, mostly in acoustics [1, 2]. The idea of applying TR in wireless communications has recently gained much attention because of its properties related to temporal and spatial focusing [3, 4]. In order to combine TR with Impulse Radio-Ultra Wide Band (IR-UWB), the use of transmission

pre-filters that convolve the UWB pulse with the channel impulse response inverted in time [5] is required. Combining TR and IR-UWB has proved to improve performance thanks to increased capacity of energy collection at the receiver [6].

The concept of TR may be applied to a network of nodes rather than a single link. As well known, the resulting system may be limited by Multi User Interference (MUI) and performance prediction requires accurate models for the MUI distribution [7, 8]. Previous investigations have highlighted several UWB peculiarities, with special focus on IR-UWB [9–12]. In particular the validity of models based on the Standard Gaussian Approximation (SGA) is questionable for UWB [13, 14].

Moving beyond acoustics, TR has also been recently proposed as an enhancement for Direction Of Arrival (DOA) estimation algorithms in solving the problem of locating active vs. passive EM targets in potentially harsh propagation environments. TR has been shown to outperform standard DOA techniques based on subspace decomposition of the received signal covariance matrix in the presence of non-homogeneous media [15, 16].

This work addresses aspects of both communication and positioning related to the combination of TR with UWB.

On the communication side, the trade-off between the number of fingers in the prefilter vs. the rake receiver is estimated, in relation with the time and space focusing properties of TR. The impact of TR on MUI distribution is then addressed, by investigating how this information can be used to adapt the receiver to the MUI distribution. The performance of the proposed adapted receiver is analyzed by means of simulations.

Based on the evidence that TR improves positioning accuracy in presence of non-homogeneous propagation media, this work investigates the possibility of introducing TR in the design of a UWB DOA positioning system. The result-

L. De Nardis (✉) · D. Panaitopol · M.-G. Di Benedetto
DIET Dept., Sapienza University of Rome, Rome, Italy
e-mail: lucadn@newyork.ing.uniroma1.it

J. Fiorina
TELECOM Dept., SUPELEC, Rennes, France

D. Panaitopol
CNDS Dept., NUS, ECE, Singapore, Singapore

ing positioning accuracy is analyzed for ideal vs. frequency selective propagation media.

Communications aspects will be addressed in Sects. 2–4. In particular, Sect. 2 defines the signal model, while Sect. 3 discusses the impact of number of fingers in the prefilter and rake receiver on signal characteristics. Section 4 focuses on MUI modeling in the case of a TR IR-UWB system. Section 5 addresses the positioning aspects by discussing performance of subspace decompositions. Finally, Sect. 6 concludes the paper.

2 Signal model

In this paper a TH-IR-UWB (Time Hopping Impulse Radio Ultra Wide Band) signal using PAM (Pulse Amplitude Modulation) as well as PPM (Pulse Position Modulation) is considered. The classical (no TR) IR-UWB signal with PAM may be written as:

$$s_{noTR}(t) = \sqrt{E_s} \sum_m a_m w(t - mT_f - c_m T_c). \quad (1)$$

In this expression, $w(t)$ is the unit-energy basic pulse waveform with a time support included in $[0, T_c]$, E_s is the energy sent per pulse, a_m the information symbol at symbol interval m , having its values in the set $\{-1, 1\}$. The frame time is $T_f = N_h T_c$, where T_c is the chip time interval (N_h is the frame length in chips). The TH code is represented by the sequence $(c_l)_{l \in \mathbb{Z}}$, the elements of which belong to $\{0, \dots, N_h - 1\}$.

The classical (no TR) IR-UWB signal with PPM may be written as:

$$s_{noTR}(t) = \sqrt{E_s} \sum_m w\left(t - mT_f - c_m T_c - d_{ppm} \left(\frac{a_m + 1}{2}\right)\right), \quad (2)$$

where d_{ppm} is the time shift used by PPM.

A multipath channel $h(t)$ will be considered in the following, defined as:

$$h(t) = \sum_{i=1}^L \gamma_i \delta(t - \tau_i), \quad (3)$$

with L be the total number of paths in the channel, τ_i the delay of the i th path and γ_i its amplitude.

By considering, without loss of generality, a PAM signal, the received signal without TR may be written as follows:

$$r_{noTR}(t) = \sqrt{\frac{E_r}{A}} \sum_m a_m h(t) * w(t - mT_f - c_m T_c) + n(t), \quad (4)$$

where $A = \int |h(t) * w(t)|^2 dt$ and E_r is the energy received per pulse. $n(t)$ is the Additive White Gaussian Noise (AWGN).

The principle of TR is to convolve the pulse by an inverted version of the channel impulse response before sending it. The propagation of the signal through the channel has therefore the effect to receive the channel response correlated with itself (thus simulating a correlation receiver). With TR the transmitted signal can be written as:

$$s(t) = \sqrt{\frac{E_s}{\int |h_{in}(t) * w(t)|^2 dt}} \times \sum_m a_m h_{in}(t) * w(t - mT_f - c_m T_c), \quad (5)$$

where E_s is still the energy sent by pulse and $h_{in}(t)$ is the prefilter. In case of perfect TR (or *full* TR) one has $h_{in}(t) = h(-t)$. To reduce the complexity of the transmitter one can use a *partial* TR by reducing the number of paths considered in $h_{in}(t)$, i.e. by selecting only the N_{in} strongest paths of $h(t)$ ($N_{in} = 1$ is equivalent to no TR):

$$h_{in}(t) = \sum_{i=1}^{N_{in}} \gamma'_i \delta(-(t - \tau'_i)), \quad (6)$$

where τ'_i and γ'_i are the delay and amplitude of the strongest paths.

The received signal is then:

$$r(t) = \sqrt{\frac{E_r}{\int |h(t) * h_{in}(t) * w(t)|^2 dt}} \times \sum_m a_m h(t) * h_{in}(t) * w(t - mT_f - c_m T_c) + n(t), \quad (7)$$

where one can define $g(t) = h(t) * h_{in}(t)$ as the equivalent TR channel, obtained as the concatenation of the transmission pre-filter and the multipath channel.

At the receiver side, a rake receiver can be used. A rake receiver performs the correlation of the received signal with a template $v(t)$. Without TR, the rake receiver output for symbol n may be written as:

$$r_{noTR}[n] = \int_t r_{noTR}(t) \cdot v_{noTR}(t - n \cdot T_f - c_n T_c) dt \quad (8)$$

For a one finger rake receiver, one has $v_{noTR}(t) = w(t)$ for a PAM signal, and $v_{noTR}(t) = w(t) - w(t - d_{ppm})$ for a PPM signal. For an all rake receiver one has $v_{noTR}(t) = h(t) * w(t)$ for a PAM signal, and $v_{noTR}(t) = (h(t) * (w(t) - w(t - d_{ppm})))$ for a PPM signal. For a partial rake receiver one has $v_{noTR}(t) = h_{out}(t) * w(t)$ for a PAM signal, and

$v_{noTR}(t) = (h_{out}(t) * (w(t) - w(t - d_{PPM})))$ for a PPM signal, where $h_{out}(t)$ is a subselection of the N_{out} strongest paths of $h(t)$.

When TR is introduced, the rake receiver output for symbol n may be written as follows:

$$r[n] = \int_t r(t) \cdot v(t - n \cdot T_f - c_n T_c) dt \quad (9)$$

For a one finger rake receiver, one has $v(t) = w(t)$ for a PAM signal, and $v(t) = w(t) - w(t - d_{PPM})$ for a PPM signal. For an all rake receiver one has $v(t) = g(t) * w(t)$ for a PAM signal, and $v(t) = (g(t) * (w(t) - w(t - d_{PPM})))$ for a PPM signal, with $g(t) = h(t) * h_{in}(t)$. For a partial rake receiver one has $v(t) = h_{out}(t) * w(t)$ for a PAM signal, and $v(t) = (h_{out}(t) * (w(t) - w(t - d_{PPM})))$ for a PPM signal, where $h_{out}(t)$ is a subselection of the N_{out} strongest paths of $g(t)$.

It can be noted that the case $N_{in} = 1$ and $N_{out} = all$ (no TR and all rake) is equivalent to the case $N_{in} = all$ and $N_{out} = 1$ (full TR and one finger rake) in terms of SNR at the rake receiver output, for same energy per symbol E_s . As a matter of fact, by considering symbol $n = 0$ and PAM, without loss of generality, the output of the rake receiver in the case $N_{in} = 1$ and $N_{out} = all$ is:

$$r[0] = \left[\left(\sqrt{\frac{E_s}{\int |h_{in}(t) * w(t)|^2 dt}} \right) \times h_{in}(t) * w(t) * h(t) + n(t) \right] * h_{out}(-t) * w(-t) \Big|_0, \quad (10)$$

where the 0 between parentheses means that the preceding function resulting from the convolution is evaluated in 0. By dividing amplitude by $\sqrt{\int |h_{out}(t) * w(t)|^2 dt}$, in order to normalize the noise component, one obtains (11), showing that taking $h_{in}(t) = h(-t)$ and $h_{out}(t) = \delta(t)$ is equivalent to taking $h_{in}(t) = \delta(t)$ and $h_{out}(t) = h(t)$.

$$r[0] = \frac{\sqrt{E_s}}{\sqrt{\int |h_{in}(t) * w(t)|^2 dt} \cdot \int |h_{out}(t) * w(t)|^2 dt} \times h_{in}(t) * h_{out}(-t) * h(t) * w(t) * w(-t)(0) + n(t) * \frac{h_{out}(-t) * w(-t)}{\sqrt{\int |h_{out}(t) * w(t)|^2 dt}}(0). \quad (11)$$

The above observation is the reason why TR is often used without a rake receiver (i.e. with a one finger rake receiver): TR is equivalent to a classical communication system with an all rake receiver, with complexity shifted from the receiver to the transmitter. The all rake receiver

is replaced by a full TR pre-filter at the transmitter although in order to increase performance, one can still use a multifinger rake receiver with TR, and trade-offs in complexity between transmitter and receiver can be achieved by tuning the number of fingers of prefilter and rake receiver.

3 On the energy concentration and on the rake receiver

3.1 Time and space focusing

The first noticeable effect of TR on the UWB signal is that it focuses the energy in time and space. The focusing in time is of particular interest for IR-UWB. As a matter of fact, IR-UWB is primarily designed to work with focused pulses in time (i.e. ultra short pulses). Due to the multipath channel, pulses that are focused in time at the transmitter ($w(t)$) may, however, arrive as spread in time at the receiver. The time focusing ability of TR can be used to refocus the pulse in time at the receiver side. TR is however able to focus the signal in time only at one receiving geographical position at a time (space focusing property). In order to focus the signal in time at receiver 1 where the channel from the transmitter is $h_1(t)$, when applying TR the transmitter must send $h_1(-t) * w(t)$ instead of transmitting the pulse $w(t)$. The received signal at receiver 1 is thus $h_1(t) * h_1(-t) * w(t)$. Due to the correlation peak of $h_1(t) * h_1(-t)$, the received pulse $h_1(t) * h_1(-t) * w(t)$ is focused in time, contrarily to the received pulse without TR ($h_1(t) * w(t)$) that is spread in time. On the other hand, for a second receiver, called receiver 2, at a different geographical position, where the channel from the transmitter is $h_2(t)$, the received signal is $h_2(t) * h_1(-t) * w(t)$. The intercorrelation $h_2(t) * h_1(-t)$ does not show any peak when the two channels are different, due to the different locations of the receivers. The signal at receiver 2 is thus not focused in time.

In addition to the time and space focusing property, TR can also lead to an energy gain thanks to the coherent combining of the channel paths. This gain appears in two ways: TR relatively increases the available received power at the position of receiver 1 with respect to other positions, but for the same transmit power it also increases the total available received power at the position of receiver 1, with respect to the total available received power at the receiver 1 without TR.

To show that TR increases the available received power at the receiver 1 position vs. other positions, one can note that at receiver 1, for a transmitted pulse $w(t) * h_1(-t)$, the received pulse $w(t) * h_1(-t) * h_1(t)$ has an energy $\int |W(f)|^2 |H_1(f)|^4 df$ (where $W(f)$ and $H_1(f)$ are the Fourier Transforms of $w(t)$ and $h_1(t)$ respectively), while at receiver 2, for a transmitted pulse $w(t) * h_1(-t)$ the received pulse $w(t) * h_1(-t) * h_2(t)$ has an energy

$\int |W(f)|^2 |H_1(f)|^2 |H_2(f)|^2 df$. Without loss of generality, one can consider that receivers 1 and 2 are at the same distance from the transmitter so that the statistical average received power without TR is the same in the two positions:

$$\begin{aligned} E \left[\int |W(f)|^2 |H_1(f)|^2 df \right] \\ = E \left[\int |W(f)|^2 |H_2(f)|^2 df \right], \end{aligned} \quad (12)$$

since $h_1(t)$ and $h_2(t)$ have the same statistical properties. Having the classical Cauchy-Schwarz inequality:

$$\begin{aligned} \int |W(f)|^2 |H_1(f)|^2 |H_2(f)|^2 df \\ \leq \sqrt{\int |W(f)|^2 |H_1(f)|^4 df} \\ \times \sqrt{\int |W(f)|^2 |H_2(f)|^4 df}, \end{aligned} \quad (13)$$

one can take the expectation:

$$\begin{aligned} E \left[\int |W(f)|^2 |H_1(f)|^2 |H_2(f)|^2 df \right] \\ \leq E \left[\sqrt{\int |W(f)|^2 |H_1(f)|^4 df} \right. \\ \left. \times \sqrt{\int |W(f)|^2 |H_2(f)|^4 df} \right], \end{aligned} \quad (14)$$

and, by assuming that $h_1(t)$ and $h_2(t)$ are independent, one has:

$$\begin{aligned} E \left[\int |W(f)|^2 |H_1(f)|^2 |H_2(f)|^2 df \right] \\ \leq E \left[\sqrt{\int |W(f)|^2 |H_1(f)|^4 df} \right] \\ \times E \left[\sqrt{\int |W(f)|^2 |H_2(f)|^4 df} \right]. \end{aligned} \quad (15)$$

By remembering that $h_1(t)$ and $h_2(t)$ have the same statistical properties one obtains:

$$\begin{aligned} E \left[\sqrt{\int |W(f)|^2 |H_1(f)|^4 df} \right] \\ = E \left[\sqrt{\int |W(f)|^2 |H_2(f)|^4 df} \right], \end{aligned} \quad (16)$$

so that:

$$\begin{aligned} E \left[\int |W(f)|^2 |H_1(f)|^2 |H_2(f)|^2 df \right] \\ \leq E \left[\sqrt{\int |W(f)|^2 |H_1(f)|^4 df} \right]^2 \\ \leq E \left[\int |W(f)|^2 |H_1(f)|^4 df \right]. \end{aligned} \quad (17)$$

Equation (17) states that statistically, even if the distances from transmitter to receivers 1 and 2 are the same, the energy received at the position of receiver 1 is greater than the one received at the position of receiver 2. One can conclude thus that, thanks to TR, not only the energy is focused in time at the position of receiver 1, but also the total available energy is greater in that specific position.

One can also determine the gain in energy brought by TR with respect to the non TR case at the same position. Call $P_{r,noTR}$ the power of the received signal at receiver 1 position without TR. When TR is introduced, the power of the received signal at the same receiver 1 position can be written as:

$$P_r = \frac{\int |W(f)|^2 |H_1(f)|^4 df \int |W(f)|^2 df}{\left(\int |W(f)|^2 |H_1(f)|^2 df \right)^2} P_{r,noTR}. \quad (18)$$

By using once again the Cauchy-Schwarz inequality one finds:

$$\frac{\int |W(f)|^2 |H_1(f)|^4 df \int |W(f)|^2 df}{\left(\int |W(f)|^2 |H_1(f)|^2 df \right)^2} \geq 1, \quad (19)$$

and thus:

$$P_r \geq P_{r,noTR}. \quad (20)$$

For the same transmit power, the introduction of TR leads therefore to an increase in received power.

The energy gain was quantified by simulation using the IEEE 802.15.3a LOS UWB channel model [17]. A chip time $T_c = 2$ ns was chosen, and the classical Scholtz's pulse was adopted for the transmitted pulse $w(t)$ [18]:

$$w(t) = \left[1 - 4\pi \left(\frac{t}{T_c} \right)^2 \right] \cdot \exp \left[-2\pi \left(\frac{t}{T_c} \right)^2 \right]. \quad (21)$$

The results are reported in the last line of Table 2 ($N_{in} = 1$ corresponds to no TR, $N_{in} = all$ corresponds to full TR).

By considering the signal sent to receiver 1 as interference for receiver 2, one can see how TR may help in reducing MUI when the interference is caused by signals meant at other positions. Without TR, if a signal has to be received with power P_1 at receiver 1, it will be received with power

I_1 at receiver 2. With TR the signal will be sent with a power divided by $\frac{\int |W(f)|^2 |H_1(f)|^4 df \int |W(f)|^2 df}{(\int |W(f)|^2 |H_1(f)|^2 df)^2} \geq 1$ in order to be received with same power P_1 (less power has to be spent by the transmitter). The signal received at receiver 2 will therefore have a power lower than I_1 , thus reducing the impact of MUI thanks to the introduction of TR.

The analysis of the impact of TR on MUI will be extended in Sect. 4 by considering a scenario characterized by different unsynchronized interfering users transmitting to the same receiver position (e.g. a base station), focusing their signals to the same point in space.

3.2 Rake receiver

The discussion on the received energy gain brought by TR which has been done in Sect. 3.1 considers the total available energy at the receiver. However, the capability of fully collecting the available energy requires the introduction of an all rake receiver. This last point is slightly in contradiction with one of the advantages of TR mentioned at the end of Sect. 2, that is the time focusing of the signal. The time focusing of the signal lets envisage that the receiver will not need a lot of fingers in a rake receiver, as the fingers are made to collect a signal spread in time. However, the time focus property of TR leads to two distinct effects: on one hand, there is a concentration of the energy on the main paths of $h_1(-t) * h_1(t)$, while on the other hand there is a larger spreading in time of the residual energy, since $h_1(-t) * h_1(t)$ has more paths and is more spread than $h_1(t)$ alone. In short, the total available energy in TR is more spread in time but the main part of this energy is less spread. In order to collect the main part of the energy, less fingers will be needed in TR than without TR, but in order to collect the total available energy, more fingers will be needed with TR than without TR.

The effect of introducing TR can be quantified by defining the efficiency of the rake receiver as the ratio between the energy per pulse captured by the receiver and the total energy available at the receiver input as a function of the number of fingers in the pre-filter and in the rake receiver, that is:

$$\text{Efficiency}(N_{in}, N_{out}) = E_r(N_{in}, N_{out}) / E_r(N_{in}, All). \quad (22)$$

Table 1 reports efficiency values obtained by simulation of a IEEE 802.15.3 channel model [17]. The complexity of implementation of a rake receiver is linked with its number of fingers. The complexity of the TR transmitter as well increases as the number of fingers in the prefilter increase (partial TR). Therefore, the complexity of a full rake receiver is greater with TR than without TR. One can clearly see from Table 1 that in order to achieve 100% efficiency, TR must use a complex receiver. Note, however, that since in TR the

Table 1 Efficiency: energy per pulse captured by the receiver, with respect to the energy really available at the receiver input ($E_r(N_{in}, N_{out}) / E_r(N_{in}, N_{out} = all)$)

N_{out}	$N_{in} = 1$	$N_{in} = 10$	$N_{in} = 20$	$N_{in} = all$
1	14.8%	37.8%	45.4%	52%
10	55%	56.7%	59.8%	62.8%
20	75.2%	65.2%	67.9%	69.12%
all	100%	100%	100%	100%

Table 2 Efficacy: energy per pulse captured by the receiver, with respect to the available energy at the receiver input without TR for the same sent energy ($E_r(N_{in}, N_{out}) / E_r(N_{in} = 1, N_{out} = all)$)

N_{out}	$N_{in} = 1$	$N_{in} = 10$	$N_{in} = 20$	$N_{in} = all$
1	14.8%	54.5%	75%	100%
10	55%	81.8%	98.8%	120.3%
20	75.2%	94%	112.1%	132.4%
all	100%	144.2%	165.2%	191.6%

available energy at the receiver may be higher than without TR for same transmitting power, it is appropriate to investigate the *efficacy* of the rake receiver defined as the ratio between the collected energy per pulse and the energy available without TR for same transmit power, as a function of the number of fingers in the pre-filter and in the rake receiver:

$$\text{Efficacy}(N_{in}, N_{out}) = E_r(N_{in}, N_{out}) / E_r(1, All). \quad (23)$$

Table 2 shows the efficacy values obtained by simulation. Results show that as expected a 100% efficacy is achieved when full TR is combined with a simple receiver (no rake), and that the introduction of TR leads to a net increase of the received energy for a medium-to-large number of fingers in the prefilter ($N_{in} \geq 10$), with a gain close to a factor of 2 when a full TR architecture combined with a full rake receiver is considered. Results highlight the trade-off introduced by the adoption of TR, involving the simplicity of the reception vs. a more efficient use of the available energy.

4 Impact of TR on MUI distribution

This section addresses a scenario where many unsynchronized users transmit to the same receiver (e.g. a base station) and the unsynchronized signals emitted by the users focus on the same geographical point.

In order to analyze the MUI distribution when the above users use TR, the signal model of Sect. 2 is extended as follows. A repetition code is taken into account and, therefore, with TR the signal originated by user k and received by the

common receiver can be written (PAM modulation) as follows:

$$r_k(t) = \sqrt{\frac{E_{r,k}}{\int |h_{in,k}(t) * w(t) * h_k(t)|^2 dt}} \times \sum_m \sum_{j=0}^{N_s-1} a_{m,k} h_{in,k}(t) * w(t - (mN_s + j)T_f - c_{mN_s+j,k}T_c) * h_k(t), \quad (24)$$

where N_s is the repetition factor, h_k is the channel impulse response between user k and receiver, $h_{in,k}(t)$ is user k TR pre-filter (subselection of the $N_{in,k}$ strongest path of $h_k(t)$), $c_{m,k}$ is the time hopping code of user k , $a_{m,k}$ is the m -th symbol sent by user k , and $E_{r,k}$ is the received energy per pulse. In the PPM case one can write:

$$r_k(t) = \sqrt{\frac{E_{s,k}}{\int |h_{in,k}(t) * w(t) * h_k(t)|^2 dt}} \times \sum_m \sum_{j=0}^{N_s-1} h_{in,k}(t) * w\left(t - (mN_s + j) \cdot T_f - c_{mN_s+j,k}T_c - d_{PPM}\left(\frac{a_{m,k} + 1}{2}\right)\right) * h_k(t). \quad (25)$$

In both PAM and PPM, there are N_s pulses by symbol due to the presence of the repetition code; in order to take a decision on the received symbol the rake receiver must collect N_s correlator outputs. Without loss of generality consider symbol $m = 0$ and a reception synchronized on user 1. The output of the pulse-by-pulse correlator can be thus written as:

$$r_{imp}[n] = \int_t r_x(t) \cdot v(t - n \cdot T_s - c_{1,n} \cdot T_c) dt, \quad (26)$$

where the index for user 1 has been dropped, and N_s outputs, from $r_{imp}[0]$ to $r_{imp}[N_s - 1]$, are collected in order to decide on the received symbol.

For PAM, one has $v(t) = h_{out}(t) * w(t)$, while for PPM one has $v(t) = (h_{out}(t) * (w(t) - w(t - d_{PPM})))$ where $h_{out}(t)$ is a subselection of the N_{out} strongest path of $g(t) = h(t) * h_{in}(t)$. The received signal $r_x(t)$ thus writes:

$$r_x(t) = r_1(t) + r_{MUI}(t) + n(t), \quad (27)$$

while the MUI signal is given by:

$$r_{MUI}(t) = \sum_{k=2}^K r_k(t - \Delta_k), \quad (28)$$

where Δ_k represents the relative delay of user k with respect to the reference signal of user 1, due to the absence of synchronization between the various users.

The classical receiver (adapted to Gaussian interference but not adapted to other distributions) makes a soft decision on the received bit based on the sign of $\sum_{n=0}^{N_s-1} r_{imp}[n]$. The pulse-by-pulse correlator output can be decomposed as follows:

$$r_{imp}[n] = r_{imp,u}[n] + r_{imp,MUI}[n] + r_{imp,AWGN}[n] \quad (29)$$

where:

- $r_{imp,u}[n] = \int_t r_1(t) \cdot v(t - n \cdot T_s - c_{1,n}T_c) dt$ is the useful signal contribution,
- $r_{imp,MUI}[n] = \int_t r_{MUI}(t) \cdot v(t - n \cdot T_s - c_{1,n}T_c) dt$ is the MUI contribution,
- $r_{imp,AWGN}[n] = \int_t n(t) \cdot v(t - n \cdot T_s - c_{1,n}T_c) dt$ is the AWGN contribution.

With reference to $r_{imp,MUI}[n]$, it has been proved that its distribution may not be Gaussian for several UWB transmission cases [13], and in particular for IR-UWB transmissions due to their impulsive nature [14]. In order to investigate the appropriateness of the standard Gaussian model for IR-UWB transmissions making use of TR the Kurtosis $k = \frac{E[r_{imp,MUI}[n]^4]}{E[r_{imp,MUI}[n]^2]^2} - 3$ will be considered as the reference parameter of the MUI distribution. The Kurtosis is a measure of how far a distribution is from the Gaussian distribution. The value for the normal distribution is $k = 0$.

4.1 Modeling of non Gaussian MUI

While the non Gaussianity of the MUI is a problem when a classical receiver is used, it has been shown in [19] that performance can be improved by adopting a receiver adapted to the MUI distribution. Following [19], the Generalized Gaussian was used to fit the MUI distribution. The expression of this distribution is as follows:

$$p(x) = \frac{c_1(\beta)}{\sqrt{\sigma^2}} \exp\left(-c_2(\beta) \left|\frac{x}{\sqrt{\sigma^2}}\right|^{\frac{2}{1+\beta}}\right), \quad (30)$$

with

$$c_1(\beta) = \frac{\Gamma^{\frac{1}{2}}(\frac{3}{2}(1+\beta))}{(1+\beta)\Gamma^{\frac{3}{2}}(\frac{1}{2}(1+\beta))}, \quad (31)$$

and

$$c_2(\beta) = \left(\frac{\Gamma(\frac{3}{2}(1+\beta))}{\Gamma(\frac{1}{2}(1+\beta))}\right)^{\frac{1}{1+\beta}}. \quad (32)$$

The relation between the Kurtosis k and the coefficient β is as follows:

$$k = \frac{\Gamma(\frac{5(1+\beta)}{2})\Gamma(\frac{(1+\beta)}{2})}{(\Gamma(\frac{3(1+\beta)}{2}))^2} = \aleph(\beta). \quad (33)$$

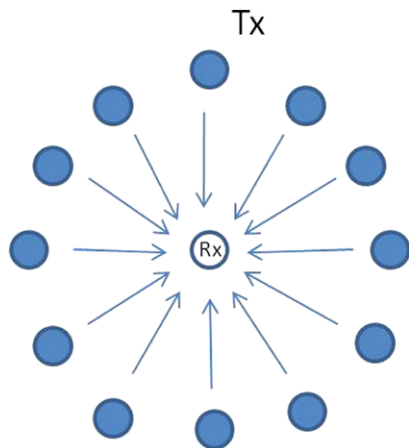


Fig. 1 Star topology

A receiver adapted to a Generalized Gaussian interference has been proposed in [20]. This receiver consists in the insertion of a non-linear limiter that takes into account the parameter $\beta = \aleph^{-1}(k)$. Then, the expression of the limiter function h_l is:

$$h_l(x) = (|x + 1|^{1+\beta} - |x - 1|^{1+\beta}). \tag{34}$$

The adapted receiver takes its decision based on the sign of $\sum_{n=0}^{N_s-1} h_l(r_{imp}[n]/E_r)$.

4.2 Simulation results

The first scenario considered 12 users distributed in the network according to a star topology (see Fig. 1), where the distance from transmitters to receiver is 10 meters. All users transmit TR PPM-TH-UWB signals at same power, while channels h_k are different among users. An IEEE 802.15.3a channel model [17] was simulated. Chip time was $T_c = 2$ ns, the PPM shift was $d_{ppm} = 0.5$ ns and the number of slots per frame was $N_h = 24$. Pulse shape $w(t)$ was, again, the Scholtz’s pulse defined in (21).

Figure 2 shows results obtained by simulating a case (a) (Fig. 2(a)) when $N_{in} = 10$ and $N_{out} = 20$, and a case (b) (Fig. 2(b)) when $N_{in} = 20$ and $N_{out} = 20$. The Kurtosis was $k = 1.42$ vs. $k = 2.37$ for case (a) vs. case (b), respectively. This result indicates that by increasing the number of fingers in the pre-filter, the Kurtosis departs from 0, that is the MUI distribution departs from a Gaussian.

A second analyzed scenario is shown in Fig. 3 and corresponds to a ring topology. This topology has been introduced in [21] as a “worst case”; the useful transmitter (user 1) is diametrically opposed to the receiver and the receiver is affected by “worst case” MUI due to the presence of dominant interferers.

System simulations adopted: $N = 30$ transmitters, a repetition code with $N_s = 6$, ring diameter set to 10 meters, symbol interval $T_s = N_h \cdot T_c = 96$ ns, chip interval $T_c = 2$ ns.

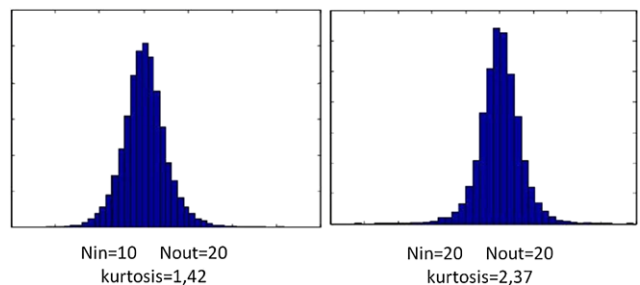


Fig. 2 Histogram of MUI ($r_{imp,MUI}$) with related kurtosis, case (a) ($N_{in} = 10$ and $N_{out} = 20$), case (b) ($N_{in} = 20$ and $N_{out} = 20$)

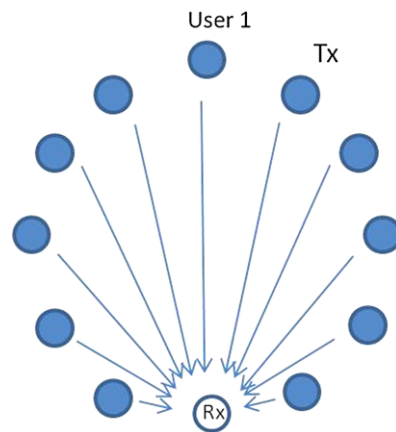


Fig. 3 Ring topology (“worst case” topology of Ref. [21])

Users transmitted at the same power. Performance evaluation was obtained by stopping simulation after 100 wrong bits were received. The $r_{imp,MUI}[n]$ distribution and the performance in terms of Bit Error Rate (BER) vs. SNR, with $N_{out} = 10$ and $N_{in} = 1, 10, 20$, all, are shown in Fig. 4. For high SNR the AWGN is negligible and performance is determined by the BER floor caused by MUI.

Figure 4 shows that when N_{in} increases (approaching full TR) the r_{MUI} distribution becomes more tight (the Kurtosis increases) and that BER decreases as the number of fingers in the TR filter increases.

Figure 5 shows, in the all rake case, the improvement of performance obtained by moving from a scheme without TR, in which a classical receiver is used, to a scheme in which a full TR configuration and a receiver adapted to a Generalized Gaussian interference are adopted, highlighting the gain brought by the exploitation of the MUI distribution change due to TR.

5 Positioning with UWB and Time Reversal

This section focuses on the application of TR combined with UWB to positioning, addressing the potential impact of TR and UWB on positioning accuracy in presence of harsh channel conditions due to frequency selective and

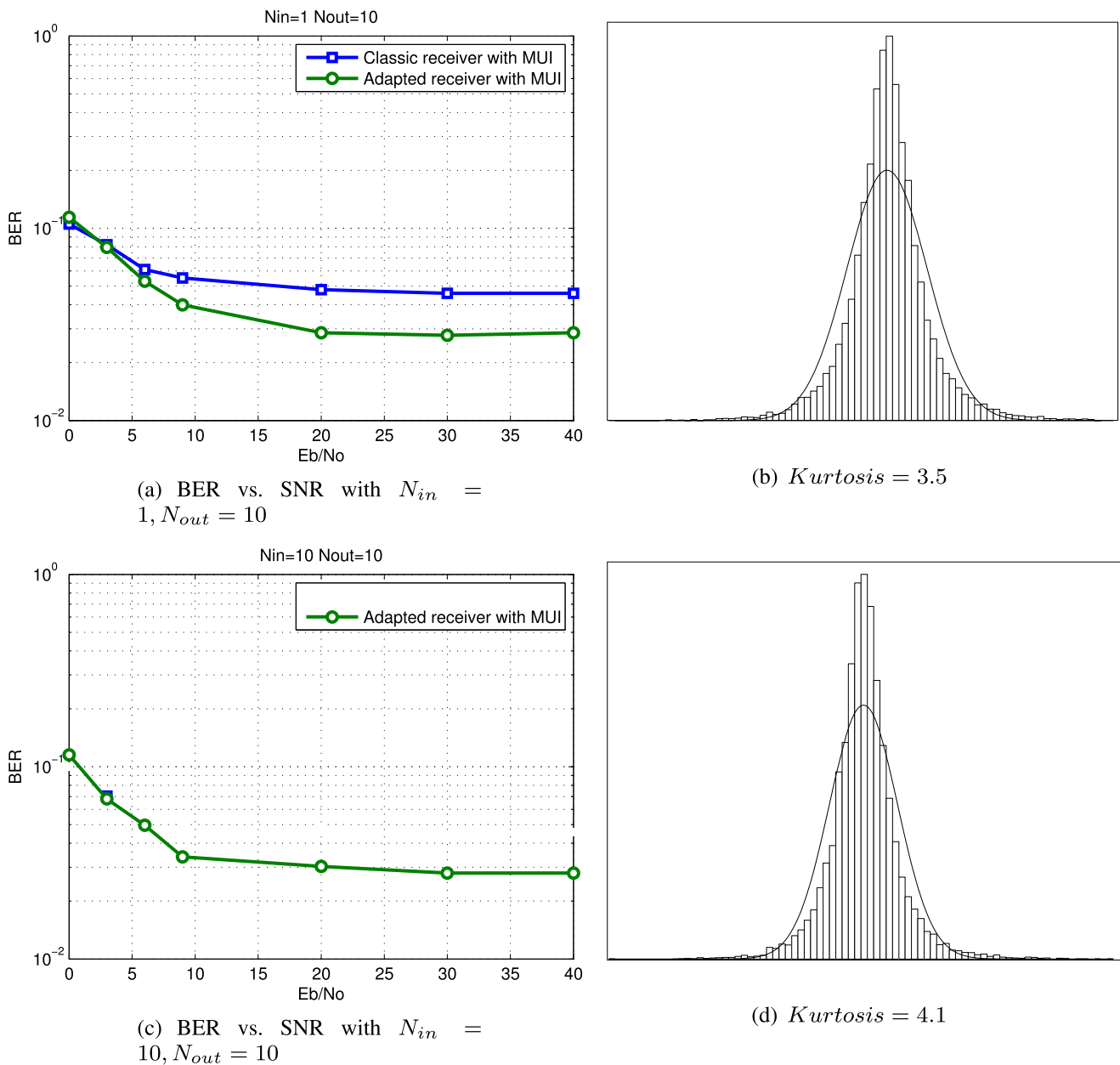


Fig. 4 Bit Error Rate (left) and histograms showing the distribution of the MUI $r_{imp,MUI}$ with superimposed a Gaussian probability density function having same variance (right), for varying $N_{in} = 1$ (Row 1, (a)–(b): $N_{in} = 1$; Row 2, (c)–(d): $N_{in} = 10$; Row 3, (e)–(f): $N_{in} = 20$; Row 4, (g)–(h): $N_{in} = all$)

non-homogeneous propagation media. The application scenario considered in the following is presented in Fig. 6, foreseeing a positioning device equipped with an antenna array composed of m elements that applies a DOA positioning technique to determine the position of d targets in unknown positions.

5.1 Positioning based on DOA estimation

The problem of determining the angle of arrival of a signal by means of an array of antenna elements was studied

extensively by the research community. A well known approach relies on subspace decomposition of a covariance matrix built from the signal received on each antenna array element from the targets: this was the basis for the definition of the MUSIC algorithm [22], that can be briefly described as follows. Let us consider an antenna array of m elements receiving the emissions of d active targets. The signal received by the i -th element of the array can be written as:

$$r_i(t) = \sum_{k=1}^d s_k(t) a(i, \theta_k) + n_i(t) \quad (35)$$

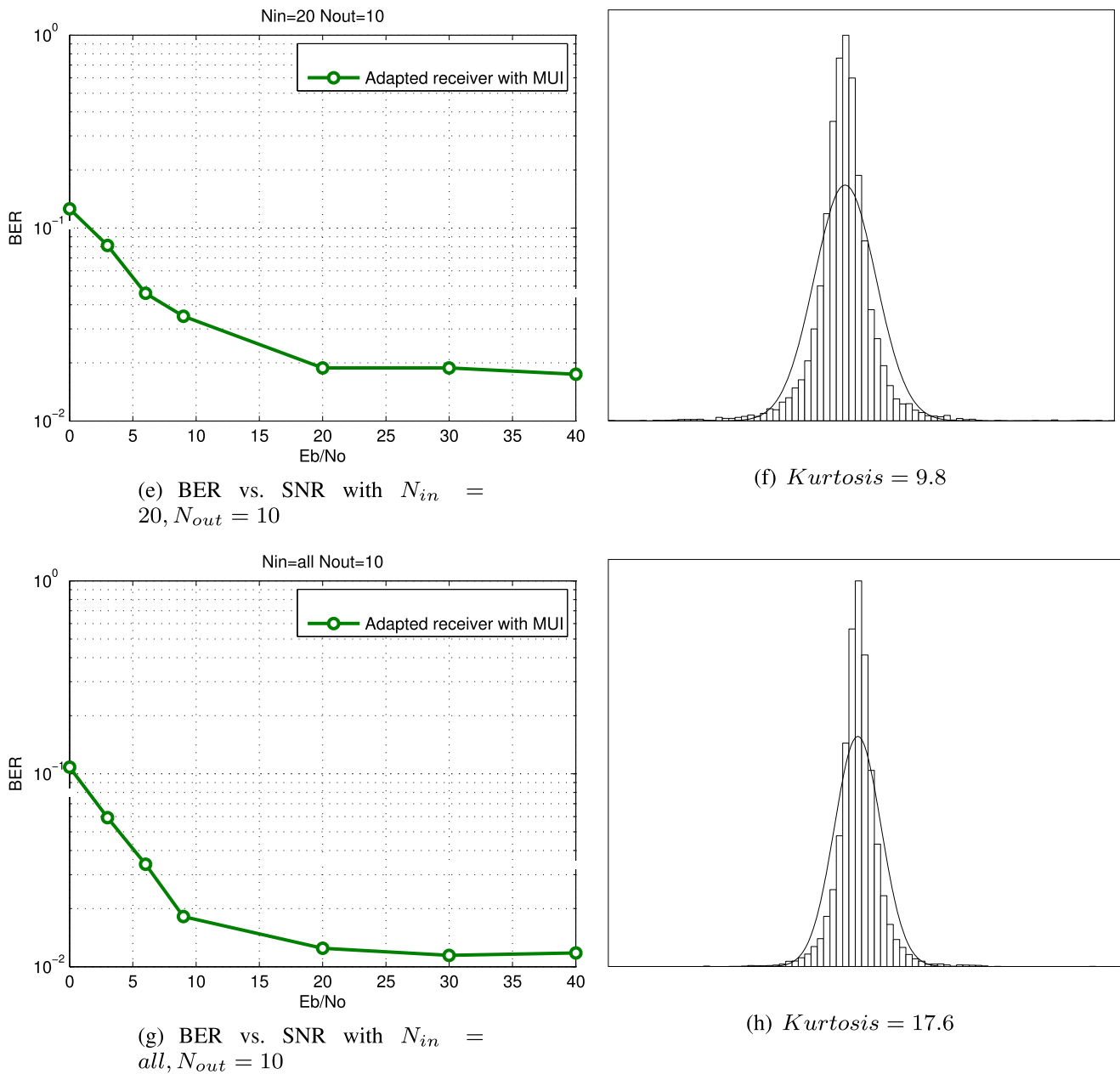


Fig. 4 (Continued)

where $s_k(t)$ is the signal emitted by target k , $a(i, \theta_k)$ is a steering function, describing the effect of the propagation in the considered medium of the signal emitted by target k from the position of the target to the i -th array element and $n_i(t)$ represents noise present at the i -th element.

Moving to the frequency domain one has the following matrix representation (where the dependence from frequency is omitted):

$$\mathbf{R} = \mathbf{A} \cdot \mathbf{S} + \mathbf{N} \quad (36)$$

where \mathbf{R} is a $m \times 1$ vector representing the signal at each array element, \mathbf{A} is a $m \times d$ matrix representing the values

of the steering functions, \mathbf{S} is a $d \times 1$ vector representing the incident signals and finally \mathbf{N} is a $m \times 1$ vector representing the noise introduced at each array element.

The MUSIC algorithm uses the information present in the matrix \mathbf{R} by evaluating the covariance matrix \mathbf{C} defined as:

$$\begin{aligned} \mathbf{C} &= \mathbf{E}[\mathbf{R} \cdot \mathbf{R}^*] \\ &= \mathbf{A} \mathbf{E}[\mathbf{S} \cdot \mathbf{S}^*] \mathbf{A}^* + \mathbf{E}[\mathbf{N} \cdot \mathbf{N}^*] \\ &= \mathbf{A} \mathbf{E}[\mathbf{S} \cdot \mathbf{S}^*] \mathbf{A}^* + \lambda \mathbf{C}_0, \end{aligned} \quad (37)$$

where it is assumed that signals and noise are uncorrelated.

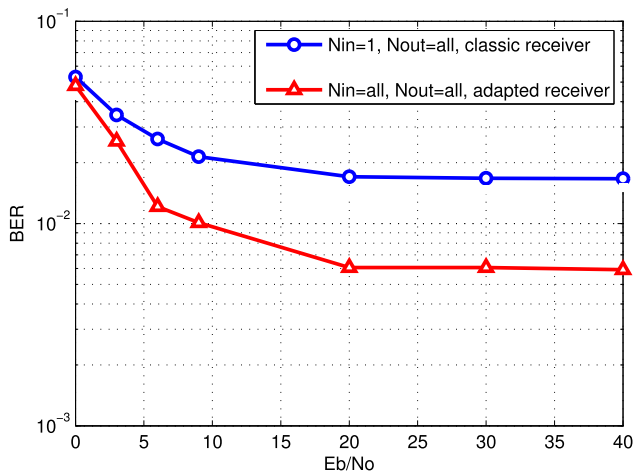


Fig. 5 BER vs. SNR with classic all rake and adapted receiver in the cases of absence of TR ($N_{in} = 1, N_{out} = all$) and complete TR configuration ($N_{in} = all, N_{out} = all$)

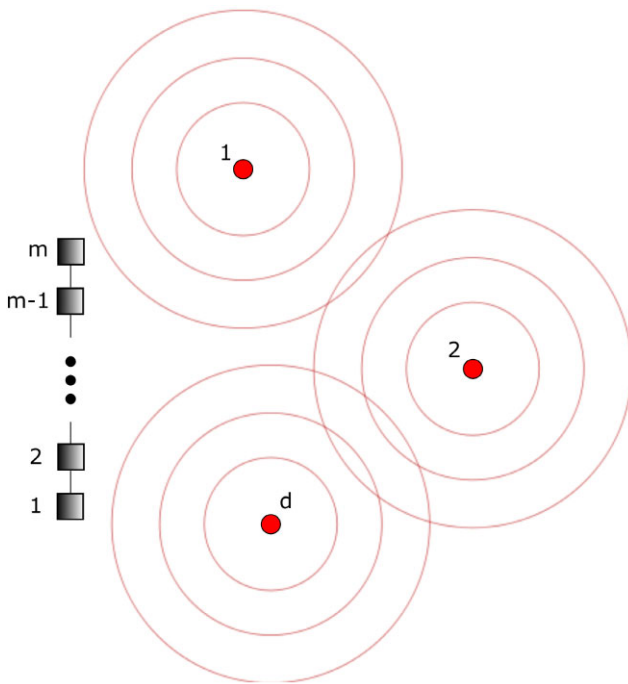


Fig. 6 Application scenario considered in the analysis of the application of UWB and TR to positioning

As long as the condition $m > d$ is verified, \mathbf{C} is a singular matrix, leading to:

$$\det(\mathbf{C}) = \det(\mathbf{A}\mathbf{E}[\mathbf{S} \cdot \mathbf{S}^*]\mathbf{A}^* + \lambda\mathbf{C}_0) = 0. \tag{38}$$

Note that in the special case where noise is characterized by zero mean and variance σ^2 one has $\lambda = \sigma^2$. As shown in [22], due to the properties of the \mathbf{S} and \mathbf{A} matrices, (38) is only solved by choosing λ as the smallest eigenvalue of the \mathbf{S} matrix λ_{min} ; furthermore such smallest eigenvalue will have

a multiplicity equal to $n = m - d$. In turn, this leads to the conclusion that there will be n eigenvectors $\{\mathbf{e}_{d+1}, \dots, \mathbf{e}_m\}$ of \mathbf{C} associated to λ_{min} that will verify the condition:

$$\mathbf{A}\mathbf{E}[\mathbf{S} \cdot \mathbf{S}^*]\mathbf{A}^* \cdot \mathbf{e}_i = \mathbf{A}^* \cdot \mathbf{e}_i = 0 \quad i = d + 1, \dots, m, \tag{39}$$

meaning that such eigenvectors define a subspace (referred to as the *noise subspace*) orthogonal to the subspace defined by the columns of the \mathbf{A} matrix. The values $\theta_1, \dots, \theta_d$ of the d angles of arrival can be then identified by defining the function:

$$P_{MU} = \frac{1}{\mathbf{a}^*(\theta)\mathbf{E}_n \cdot \mathbf{E}_n^*\mathbf{a}(\theta)} \tag{40}$$

where $\mathbf{E}_n = [\mathbf{e}_{d+1}, \dots, \mathbf{e}_m]$. The function is usually referred to as *MUSIC pseudospectrum*, and its peaks as it varies as a function of θ reveal the direction of arrival of the d signals.

5.2 Time Reversal application to positioning

The MUSIC approach presented above works well when the function $a(\theta)$ provides an accurate description of the relation between the angle of arrival θ and the signal present at each array element. This is the case for homogeneous propagation media, for which a very good approximation of the impact on each array of a signal coming from an arbitrary point in space can be achieved by means of planar wave assumption. In the case of non-homogeneous media the MUSIC approach applied to the covariance matrix leads to poor results, due to the lack of accuracy of the $a(\theta)$ function in modeling the propagation of the signals. Several authors [16, 23] pointed out that good positioning results can be achieved by applying the subspace decomposition approach proposed in MUSIC to the *TR matrix* $\mathbf{T} = \mathbf{K}^*\mathbf{K}$, where \mathbf{K} is the *Multi Static Response* (MSR) matrix defined as follows:

$$\mathbf{K} = \{\mathbf{K}_{l,j}\} = \sum_{i=1}^d \mathbf{a}(\mathbf{l}, \theta_i)\mathbf{S}_i\mathbf{a}(\mathbf{j}, \theta_i), \tag{41}$$

where \mathbf{S}_i represents the amplitude at the selected frequency of the signal emitted by the i -th target.

The element (l, j) of the MSR matrix represents the effect of a signal emitted by the l -th array element on the j -th one when taking into account the reflection of such signal by the d targets. Note that this approach applies to both passive targets (scatterers) and active ones, actually receiving the signals from the array elements and re-emitting them.

The TR matrix \mathbf{T} represents in this case the result of the time reversal operation carried out by the antenna array, where the signals received from the targets are time-reversed and retransmitted. By applying the subspace decomposition approach to the \mathbf{T} matrix in place of the \mathbf{R} matrix defined in Sect. 5.1 the positions of the d targets can

be determined, with the additional advantage provided by TR of overcoming the limitations of the subspace decomposition techniques in presence of non-homogeneous media, guaranteeing thus high positioning accuracy in random media [15, 23].

5.3 The role of UWB

The adoption of UWB signals can further improve the performance of TR-based positioning. As stated before, MUSIC and TR techniques are typically applied in the frequency domain, by assuming narrow-band signals and considering a single frequency. The adoption of wide band signals can improve performance by reducing the impact of spurious peaks in the MUSIC pseudospectrum due to low SNRs of the signals arriving at the array at a specific frequency.

In particular, assuming that the signal has a bandwidth W and that the MSR matrix can be evaluated across such

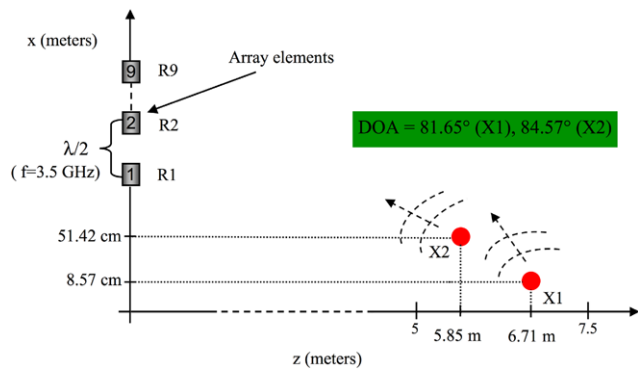


Fig. 7 Simulation scenario used as an example of application of TR and MUSIC to UWB signals

Fig. 8 DOA estimation obtained in absence of noise by applying TR and MUSIC to narrowband signals at $f = f_p$

bandwidth, the MUSIC pseudospectrum can be redefined as follows:

$$P_{TR_MU}^W = \int_W \frac{1}{\mathbf{a}^*(\theta, \mathbf{f}) \mathbf{E}_n(\mathbf{f}) \cdot \mathbf{E}_n(\mathbf{f})^* \mathbf{a}(\theta, \mathbf{f})} df. \quad (42)$$

As an example, let us consider the scenario presented in Fig. 7, where an array of 9 elements is used to determine the direction of arrival of signals emitted by two targets.

Figure 8 presents the results obtained by applying TR and MUSIC to narrowband signals at frequency $f_p = 3.5$ GHz under ideal conditions without thermal noise, and highlights the very good performance of the algorithm, with virtually error-free estimation of direction of arrival of the two signals.

Figure 9 presents the results obtained under the same hypothesis about signal bandwidth, but in presence of thermal noise and assuming a SNR of 10 dB for both signals, reduced by 10 dB due to an additional path loss introduced over a 50 MHz band centered around f_p . Figure 9 highlights the low accuracy of the algorithm under these conditions.

Finally, Fig. 10 presents the results obtained by replacing the narrowband signals with UWB signals characterized by a 500 MHz bandwidth around f_p , and by applying the frequency-averaged TR MUSIC algorithm described by (42). Results show the potential improvement achieved by taking advantage of larger bandwidths when dealing with frequency selective channels.

6 Conclusions

This work focused on two key application fields of UWB and TR: communication and positioning.

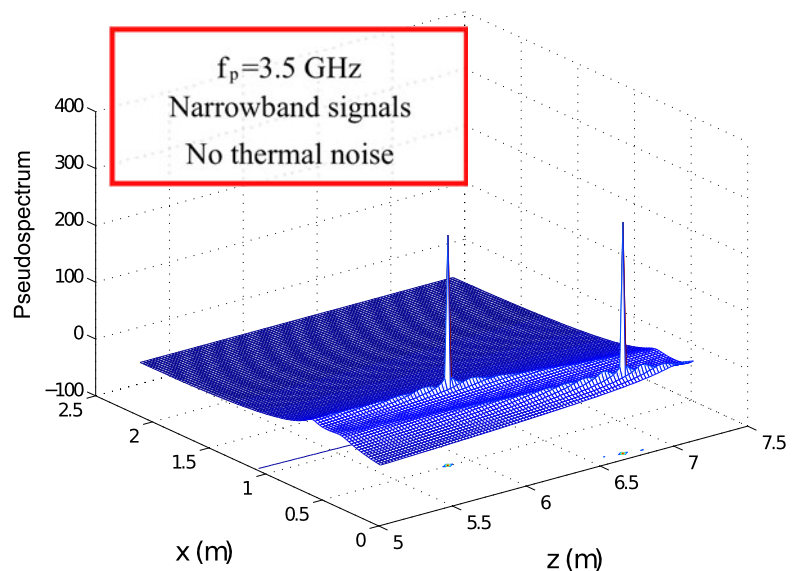


Fig. 9 DOA estimation obtained in presence of noise by applying TR and MUSIC to narrowband signals at $f = f_p$, assuming for both signals an SNR of 10 dB and an additional path loss of 10 dB over a 50 MHz frequency band centered around f_p

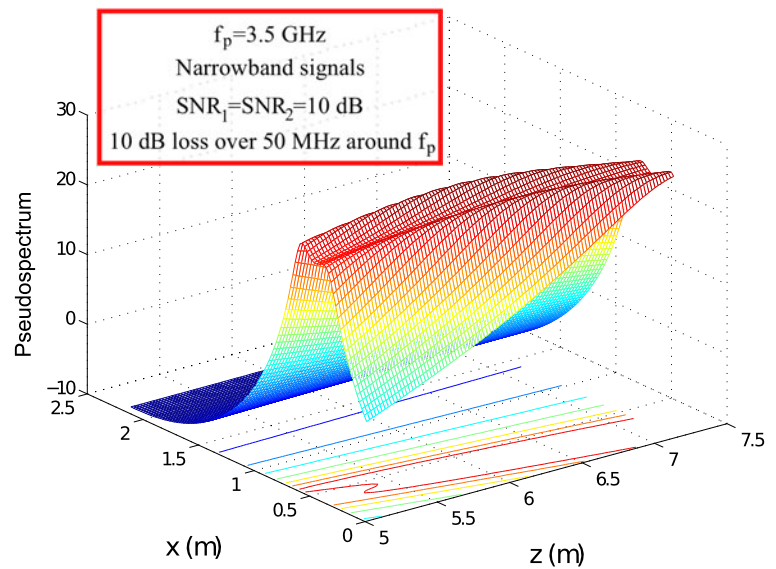
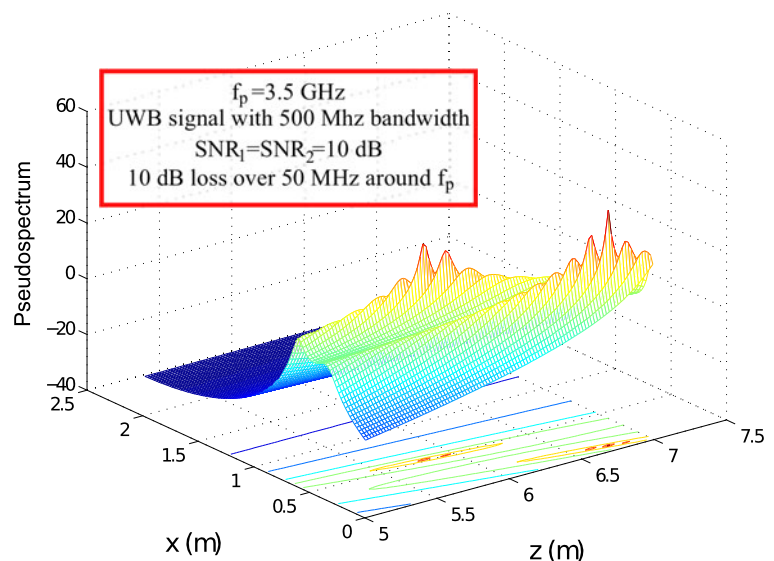


Fig. 10 DOA estimation obtained in presence of noise by applying TR and MUSIC to UWB signals with a bandwidth $W = 500$ MHz centered at $f = f_p$, assuming for both signals an SNR of 10 dB and an additional path loss of 10 dB over a 50 MHz frequency band centered around f_p



The analysis of communications related aspects showed how the focusing properties of TR can be used in UWB-IR systems. The analysis highlighted that the key parameters determining the quality of TR are the number of fingers in the transmit pre-filter and in the rake receiver (related respectively to the complexity of transmitter vs. receiver). Simulation results showed that the MUI distribution resulting from the time focusing property of TR brings significant performance improvements, in particular if a receiver adapted to such distribution is adopted.

The second part of the work focused on the study of UWB and TR in the context of positioning based on DOA estimation, and the analysis highlighted the advantages guaranteed by the introduction of TR (robustness to non-homogeneity of the propagation medium) and UWB (robustness to frequency selectivity).

Acknowledgements This work was supported in part by COST Action IC0902 “Cognitive Radio and Networking for Cooperative Coexistence of Heterogeneous Wireless Networks”. This work is inspired by the FP7-ICT 257626 NoE ACROPOLIS (Advanced coexistence technologies for radio optimisation in licensed and unlicensed spectrum) project.

The authors wish to thank Guido Capodanno for setting up the simulator and running simulation experiments.

References

1. Fink, M. (2008). Time-reversal waves and super resolution. *Journal of Physics: Conference Series* 124. 4th AIP international conference and the 1st congress of the IPIA.
2. Derode, A., Roux, P., & Fink, M. (1995). Robust acoustic time reversal with high-order multiple scattering. *Physical Review Letters*, 75, 4206–4209.
3. Abiodun, E. A., Qiu, R. C., & Guo, N. (2005). Demonstrating time reversal in ultra-wideband communications using time do-

- main measurements. In *51st International instrumentation symposium*, 8–12 May 2005, Knoxville, Tennessee.
4. Xiao, S., Chen, J., Liu, X., & Wang, B.-Z. (2008). Spatial focusing characteristics of time reversal UWB pulse transmission with different antenna arrays. *Progress in Electromagnetics Research B*, 2, 223–232.
 5. Strohmer, T., Emami, M., Hansen, J., Papanicolaou, G., & Paulraj, A. J. (2004). Application of time-reversal with MMSE equalizer to UWB communications. In *Proceedings of IEEE global telecommunications conference (GLOBECOM '04)*, Dallas, Texas, USA, November–December (vol. 5, pp. 3123–3127).
 6. Liu, X., Wang, B.-Z., Xiao, S., & Deng, J. (2008). Performance of impulse radio UWB communications based on Time Reversal technique. *Progress in Electromagnetics Research*, 79, 410–413.
 7. Di Benedetto, M.-G., De Nardis, L., Junk, M., & Giancola, G. (2005). $(UWB)^2$: uncoordinated, wireless, baseborn medium access control for UWB communication networks. *Mobile Networks and Applications*, 10(5), 663–674.
 8. Giancola, G., & Di Benedetto, M.-G. (2006). A novel approach for estimating multi user interference in impulse radio UWB networks: the pulse collision model. *Signal Processing*, 86(9), 2185–2197. Special Issue on Signal Processing in UWB Communications.
 9. Di Benedetto, M.-G., & Giancola, G. (2004). *Understanding ultra wide band radio fundamentals*. Upper Saddle River: Prentice Hall, Pearson Education.
 10. Di Benedetto, M.-G., & Vojcic, B. R. (2003). Ultra wide band (UWB) wireless communications: a tutorial. *Journal of Communications and Networks*, 5(4), 290–302, Special Issue on Ultra-Wideband Communications.
 11. De Nardis, L., & Di Benedetto, M.-G. (2003). Medium access control design for UWB communication systems: review and trends. *Journal of Communications and Networks*, 5(4), 386–393.
 12. Cardinali, R., De Nardis, L., Lombardo, P., & Di Benedetto, M.-G. (2006). UWB ranging accuracy in high- and low-data-rate applications. *IEEE Transactions on Microwave Theory and Techniques*, 54(4), 1865–1875.
 13. Durisi, G., & Romano, G. (2002). On the validity of Gaussian approximation to characterize the multiuser capacity of UWB TH-PPM. In *IEEE Conf. on Ultra Wideband Systems and Technologies*.
 14. Fiorina, J., & Hachem, W. (2006). On the asymptotic distribution of the correlation receiver output for time-hopped UWB signals. *IEEE Transactions on Signal Processing*, 54(7), 2529–2545.
 15. Borcea, L., Papanicolaou, G. C., Tsogka, C., & Berryman, J. (2002). Imaging and time reversal in random media. *Inverse Problems*, 18(5), 1247–1279.
 16. Prada, C., & Thomas, J.-L. (2003). Experimental subwavelength localization of scatterers by decomposition of time reversal operator interpreted as covariance matrix. *The Journal of the Acoustical Society of America*, 114(1), 235–243.
 17. Foerster, J. (2003). Channel modeling sub-committee report final. IEEE P802.15-02/490r1-SG3a, February.
 18. Win, M. Z., & Scholtz, R. A. (2000). Ultra-wide bandwidth time-hopping spread-spectrum impulse radio for wireless multiple-access communications. *IEEE Transactions on Communications*, 48(4), 679–691.
 19. Fiorina, J., & Domenicali, D. (2009). The non validity of the Gaussian approximation for multi-user interference in ultra wide band impulse radio: from an inconvenience to an advantage. *IEEE Transactions on Wireless Communications*, 8, 5483–5489.
 20. Fiorina, J. (2006). A Simple IR-UWB receiver adapted to multi-user interferences. In *IEEE Globecom 2006*, San Francisco, 27 Nov.–1 Dec., 2006.
 21. Domenicali, D., Giancola, G., & Di Benedetto, M.-G. (2006). Fluid coding and coexistence in ultra wide band networks. *Journal on Special Topics in Mobile Networks and Applications*, 11(4), 501–508.
 22. Schmidt, R. O. (1986). Multiple emitter location and signal parameter estimation. *IEEE Transactions on Antennas and Propagation*, AP-34(3), 276–280.
 23. Lev-Ari, H., & Devaney, A. J. (2000). The time-reversal technique re-interpreted: subspace-based signal processing for multi-static target location. In *IEEE sensor array and multichannel signal processing workshop*, Cambridge, MA, March (pp. 509–513).



Luca De Nardis received both his Laurea degree and his Ph.D. from Sapienza University of Rome in 2001 and 2005, respectively. Since December 2008 he is an Assistant Professor at the DIET Department of Sapienza University of Rome. Luca De Nardis authored or co-authored over 50 publications in international peer-reviewed journals and conferences. He is currently an Associate Editor for the Research Letters in Communications journal, published by Hindawi Publishing Corporation. He is also a reviewer for several international Journals and Transactions published by IEEE, ACM and EURASIP, and served as member of Technical Program Committee of over 30 international IEEE conferences. Since 2002, he has been participating in European IST projects focusing on Ultra Wide Band communication systems. He is presently involved in several European initiatives focusing on cognitive radio and networks, including COST Actions IC0905 (national representative for Italy) and IC0902, and the ACROPOLIS Network of Excellence. His research interests focus on UWB radio technology, Medium Access Control, routing and positioning protocols for wireless networks, and on the design of cognitive wireless networks. He is an IEEE member since 1998.



Jocelyn Fiorina was born in Paris, France, in 1976. He received the engineering degree from Ecole Supérieure d'Electricité (SUPELEC), Paris, in 2001, together with the Laurea degree in telecommunications engineering (summa cum laude) from the University of Rome, La Sapienza, Italy. In 2001, he worked as IT manager in New York, NY, for the French embassy. He obtained his Ph.D. in 2005 from the Université de Paris Sud. He is currently an Associate Professor with SUPELEC, Paris where he entered in 2002.



Dorin Panaitopol was born in Bucharest, Romania, in 1982. He received his B.Sc. Degree in September 2005 from Politehnica University of Bucharest (UPB), Faculty of Electronics, Telecommunications and Information Technology. His major degree is in the field Mobile and Satellites Communications. In 2006 he received his MASTER Degree from SUPELEC on Radiocommunications Systems. He is working towards his Joint-Ph.D. Degree with SUPELEC and NUS, on the field of UWB ad-hoc Sensor Networks.



Maria-Gabriella Di Benedetto obtained her Ph.D. in Telecommunications in 1987 from Sapienza University of Rome, Italy. In 1991, she joined the Faculty of Engineering of Sapienza University of Rome, where currently she is a Full Professor of Telecommunications. She has held visiting positions at the Massachusetts Institute of Technology, the University of California, Berkeley, and the University of Paris XI, France. In 1994, she received the Mac Kay Professorship award from

the University of California, Berkeley. Her research interests include wireless communication systems and speech. From 1995 to 2000, she

directed four European ACTS projects for the design of UMTS. Since 2000, she has been active in fostering the development of Ultra Wide Band (UWB) radio communications in Europe, and participated in several pioneering EU projects on UWB communications. More recently, participation in the European Network of Excellence HYCON (Hybrid Control: Taming Heterogeneity and Complexity of Networked Embedded Systems) offered the framework that led to increased activity in the field of cognitive networks. Professor Di Benedetto currently coordinates COST Action IC0902 'Cognitive Radio and Networking for Cooperative Coexistence of Heterogeneous Wireless Networks' and her research group participates in the European Network of Excellence ACROPOLIS (Advanced coexistence technologies for radio optimisation in licensed and unlicensed spectrum). In October 2009, Dr. Di Benedetto received the Excellence in Research award 'Sapienza Ricerca', under the auspices of President of Italy, Giorgio Napolitano.